# Supporting Information

## Direct Imaging of Protein Organization in an Intact Bacterial Organelle Using High-Resolution Atomic Force Microscopy

Sandip Kumar[1,4], Michaël L. Cartron[2,4], Nic Mullin[1,4], Pu Qian[2,4], Graham J. Leggett[3,4], C. Neil Hunter[2,4] and Jamie K. Hobbs[1,4*]

1. Department of Physics and Astronomy, University of Sheffield, UK
2. Department of Molecular Biology and Biotechnology, University of Sheffield, UK
3. Department of Chemistry, University of Sheffield, UK
4. Krebs Institute, University of Sheffield, UK

* E-mail: jamie.hobbs@sheffield.ac.uk

**1. Cantilever selection:** As discussed in the main text, low tip sample forces are required to minimize disruption of the chromatophore vesicles. In the work presented here, we have utilized the improvement in signal-to-noise ratio afforded by small cantilevers to allow high resolution imaging at low forces.

For tapping mode AFM, the time-averaged tip-sample force, $\langle F_{TS} \rangle$, assuming negligible tip-sample power dissipation, is given by:

$$\langle F_{TS} \rangle = \frac{k}{2Q} \sqrt{A_0^2 - A_{SP}^2}$$

where $k$ is the cantilever stiffness, $Q$ is the quality factor, $A_0$ is the free amplitude and $A_{SP}$ is the setpoint amplitude.[1-2] When working in liquid, $Q$ is reduced to near unity, therefore if low tip-sample forces are required, cantilevers with low $k$ must be used with small $A_0$ and $A_{SP}$ as close to $A_0$ as possible. Reduction of both $k$ and $A_0$ causes a conflict, as the thermal noise of the cantilever increases with decreasing $k$, with values of a few Angstroms being typical for soft AFM cantilevers. Noise in the optical lever detection system is also a significant noise source. Both of these problems may be addressed by using smaller cantilevers, which have become commercially available in the last few years.

While the RMS amplitude of the thermal noise depends only on $k$ and the temperature, smaller cantilevers have a lower effective mass and hence a higher resonant frequency for the same value of $k$. This causes the thermal noise to be spread over a larger bandwidth. In the majority of AFM systems, including the one used here, the amplitude of the cantilever oscillation is demodulated by a lock-in amplifier. This only passes noise in a limited bandwidth around the drive frequency, typically chosen close to resonance. Supplementary Figure 1a shows thermal noise spectra for 3 cantilevers with similar values of $k$, but with significantly different sizes (DNP-B, Bruker, nominal length 205 µm, measured $k$ 0.14 N/m; DNP-C, Bruker, nominal length 120 µm, measured $k$ 0.28 N/m and FastScan D, Bruker, nominal length 16 µm, measured $k$ 0.18 N/m). It is clear that the smallest cantilever has the lowest thermal noise amplitude on resonance, and that a much smaller fraction of the total thermal noise is contained within a typical imaging bandwidth (1-10 kHz) of the resonant frequency.[3]

As well as the thermal noise of the cantilever, which is concentrated at frequencies close to the cantilever resonance, there is also a white noise component, visible as a constant baseline in the noise spectra of Supplementary Figure 1a. This is due to noise in the optical lever detection system, and is also significantly reduced for smaller cantilevers. The reason for this is that the optical lever detects the angle of the upper surface of the cantilever, as opposed to its displacement. Shorter cantilevers give a greater angular displacement for a given spatial displacement of the tip, giving a larger signal at the detector and diluting the contribution of noise sources such as laser power fluctuations.

The traces shown in Supplementary Figure 1 b, d and f show the deflection trace for each of the 3 cantilevers driven at resonance in water with an amplitude of 1 nm, well above the sample surface. The reduction in noise from largest (b) to smallest (f) is striking. Supplementary Figures 1 c, e and g show the amplitude demodulated by the lock-in amplifier with a bandwidth of 1 kHz. The RMS variation in the demodulated amplitude is 0.085 nm in (c), 0.036 nm in (e) and 0.015 nm in (g). These correspond to signal-to-noise ratios of approximately 8, 20 and 47, respectively. At a signal-to-noise ratio below approximately 10, the noise in the amplitude signal is greater than the difference between the free amplitude and the setpoint used in this work, and the tip is unable to reliably track the surface.

**2. Selection of imaging amplitude:** It is intuitively expected that small amplitudes should be preferable for high resolution imaging, as the tip spends a greater fraction of its time close to the surface. Furthermore, smaller amplitudes give lower tip-sample forces if all other parameters are equal (see Supplementary Information section 1, above). Giessibl and co-workers[4] have demonstrated that the signal-to-noise ratio in FM-AFM is optimum when the amplitude is matched to the decay length of the tip-sample interaction. Assuming that the tip-sample interaction is dominated by the electrostatic double layer force, this decay length is expected to be similar to the Debye length. Under physiological conditions the Debye length is typically on the order of 1 nm, and may be tuned by varying the ionic strength of the imaging buffer (see Figure 1a, b).[5]

**3. Image processing:** To visualize the small protrusions of photosystem complexes above the curved vesicular surface of the chromatophores, the raw height images were high-pass filtered. For all the high-pass filtered AFM images, a Gaussian filter with a filter length of 25 nanometers was applied in the horizontal direction using 'Nanoscope Analysis 1.5'. The filtering improved the contrast and the LH2 and the RC-LH1-PufX complexes could be easily seen. The pixel position of the center of the photosystem complexes were then located manually in the high pass filtered images. Since the filtering only affects the height/intensity of each of the pixels and not their x, y location, the pixel location of the centers of photosystem complexes in case of the filtered image and the raw image were the same. The pixel position of the centers of the photosystem complexes and the raw height channel of the AFM images were used to make profiles along the vesicles' surface (see inset Figure 5). These profiles were further fit to a quadratic and the curve length of these fits were taken as the distance between the centers. The heights from the high-pass filtered image was not used in any calculations as the filtering

affects the pixel intensities in a non-linear fashion. To further avoid confusion, the height range of high-pass filtered images are not shown in the Figure captions.

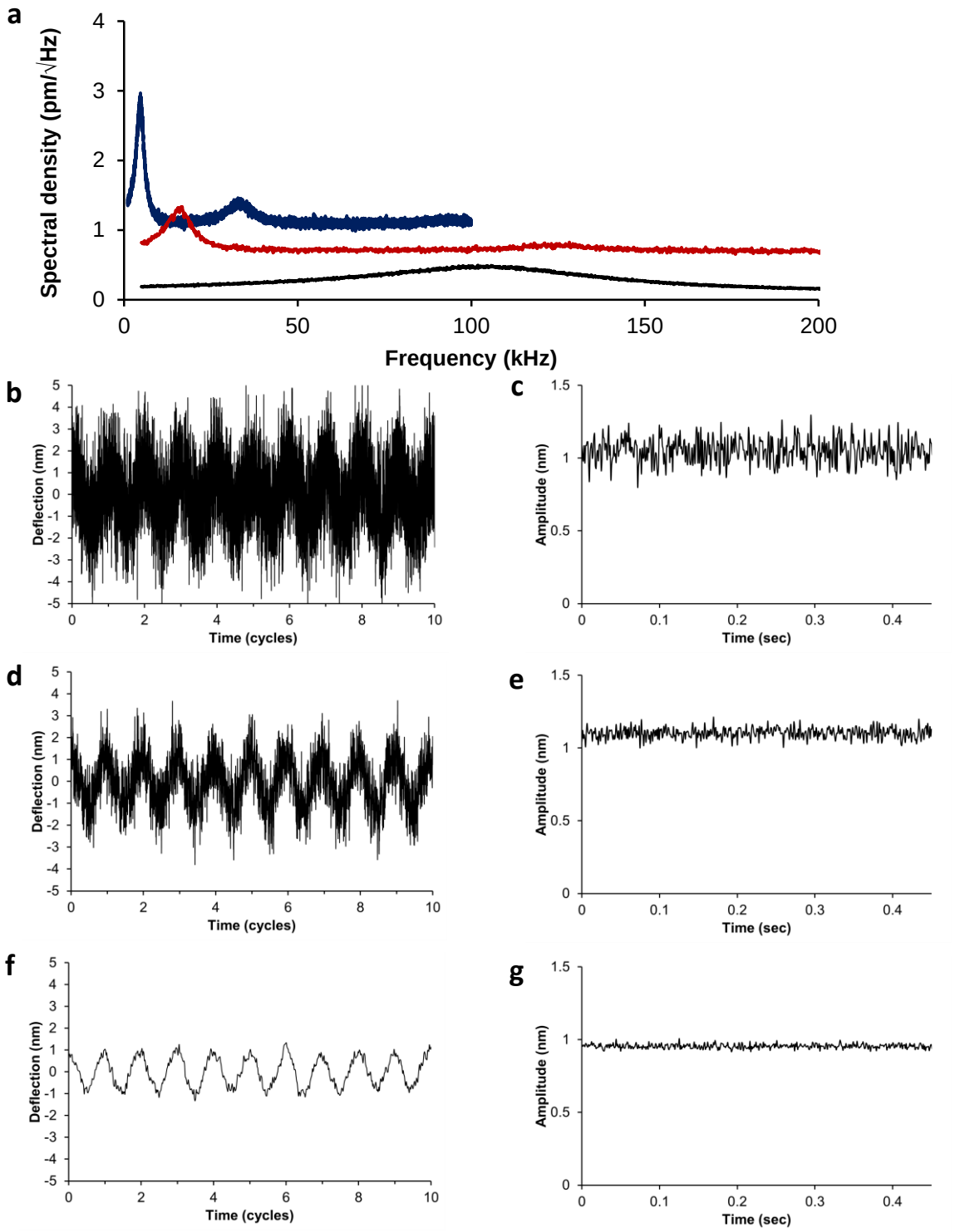


**Supplementary Figure 1. Characterization of different AFM cantilevers.** (a): calibrated thermal noise spectra for DNP-B (nominal length 205 µm, measured k 0.14 N/m, blue line); DNP-C (nominal length 120 µm, measured k 0.28 N/m, red line) and Fastscan D (nominal length 16 µm, measured k 0.18 N/m, black line). (b), (d), (f): deflection trace for a DNP-B (b), DNP-C (d) and FastScan-D (e) cantilevers, each driven at an amplitude of 1 nm, at resonance, in water, well above the sample surface. All signals were sampled at 6.25 MHz. (c), (e), (g): demodulated amplitude signals for DNP-B (c), DNP-C (e) and FastScan-D (g). All cantilevers were tuned to an amplitude of 1 nm at resonance in water. The amplitude signal was demodulated with a lock-in bandwidth of 1 kHz and sampled at 1 kHz in all cases.

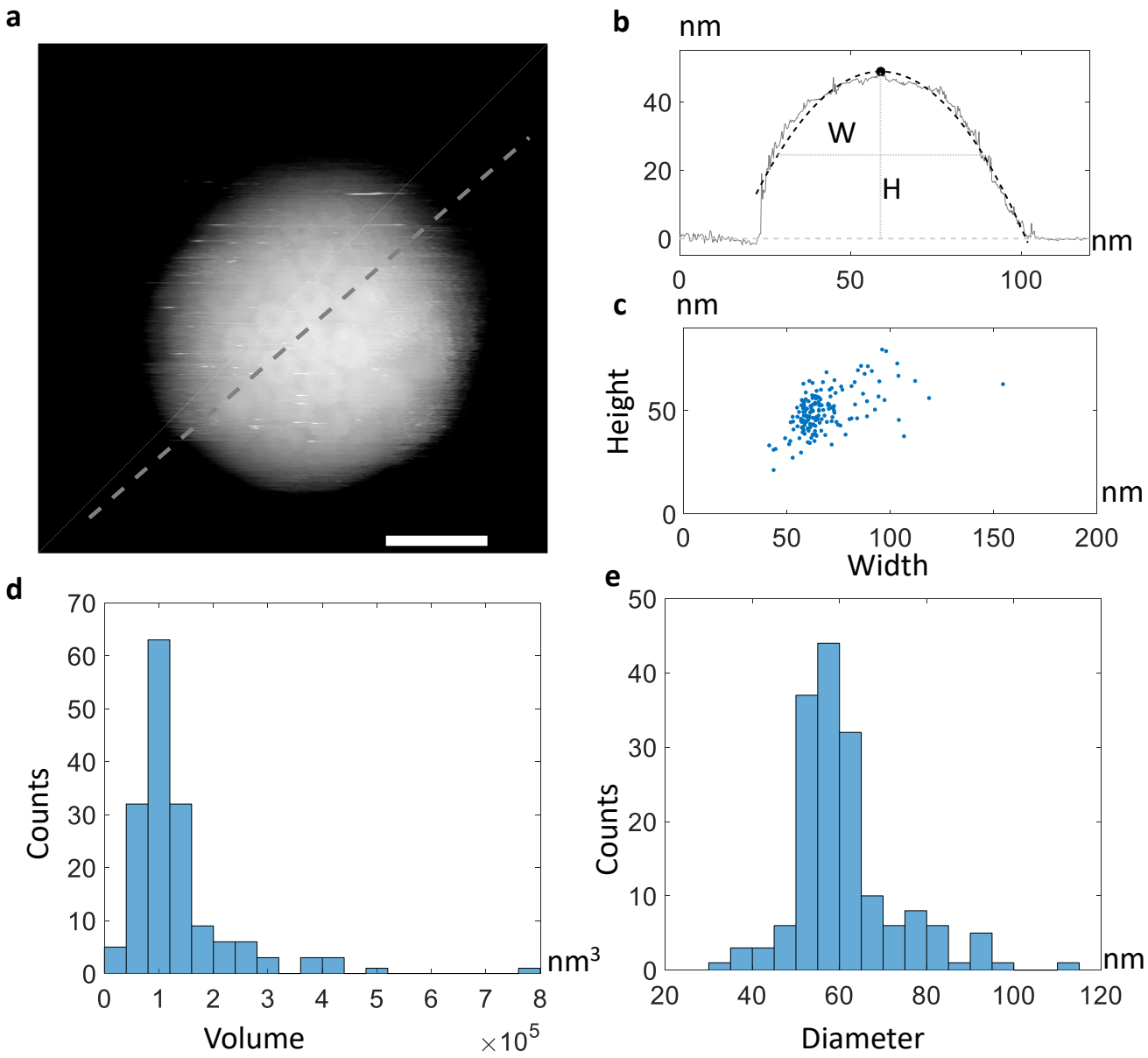


**Supplementary Figure 2. Size distribution of vesicular chromatophores.** (a) is the height image of a chromatophore vesicle. (b) is a cross sectional profile with the height (H) and width (W) marked. The background and the surface of the vesicle were each fitted with a quadratic (shown in grey and black, respectively). The maximum separation between the fitted profiles was calculated using the Matlab function "distance2curve.m" (downloaded from Matlab Central) to give H. The full width at half maximum of the fit to the chomatophore surface is W. The heights were slightly over-estimated while the widths were slightly under-estimated in the fit. Two such cross-sections were made for each chromatophore to give the maximum and minimum width. The height was taken as the average of the two heights obtained from the two fits. (c) shows the height and width of the 168 vesicular chromatophores imaged. The volume for each chromatophore was calculated using the formulae $V = \frac{\pi}{6} H W_1 W_2$ and its distribution is shown in (d). Assuming the chromatophores as spheres deformed due to immobilization, the volume conserving diameter can be calculated using the formulae (see ref. 3 in main text), $\mathrm{D} = \sqrt[3]{(\frac{6}{\pi} V)} = \sqrt[3]{H W_1 W_2}$, and the histogram in (e) shows their distribution. Scale bar in (a) represents 20 nm and black to white is 40 nm.

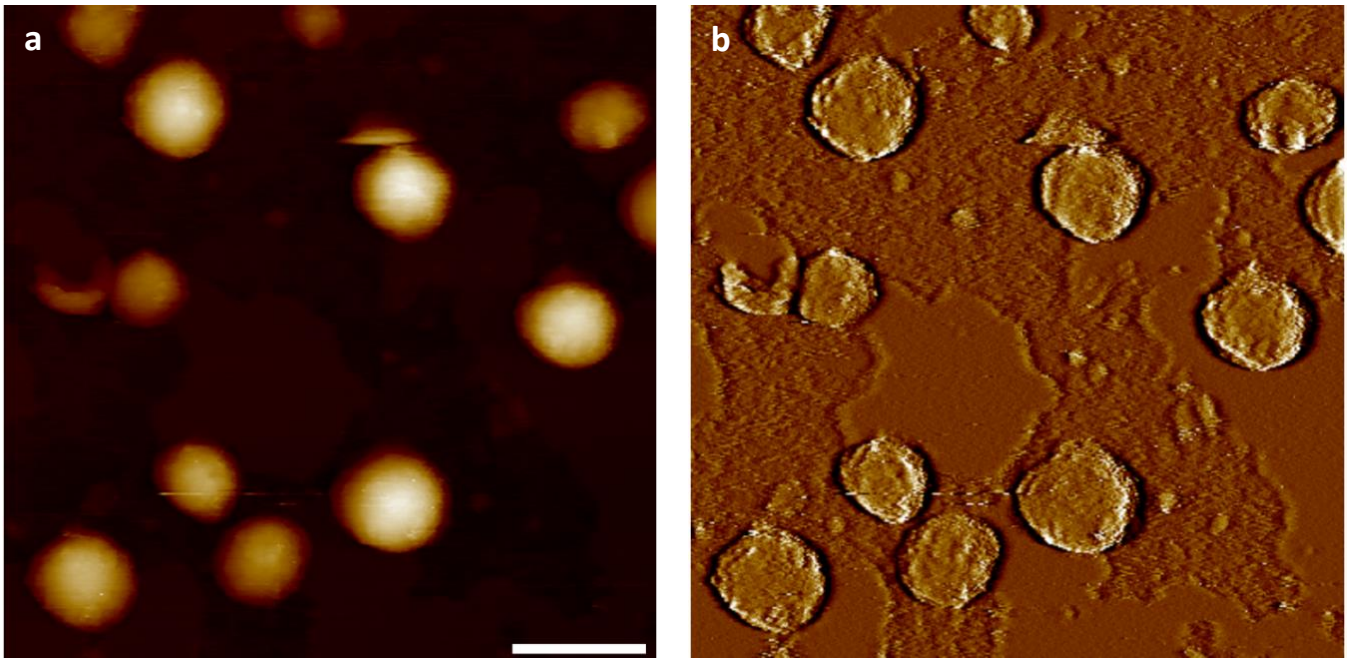


**Supplementary Figure 3. AFM scan showing multiple chromatophore vesicles immobilized onto a mica surface.** (a) shows the height image which when high-pass filtered gives image (b) (see Supplementary Information Section 3). The rough surface is mica, the smooth flat surface is the lipid bilayer and the circular objects are chromatophores. High salt buffer with divalent cations (25 mM $MgCl_2$, 150 mM KCl, and 20 mM MOPS pH7.4) was used to immobilize the chromatophore vesicles. The image shows the variation of size of chromatophore vesicles. Scale bar in (a) represents 100 nm. Black to white in (a) is 70 nm.

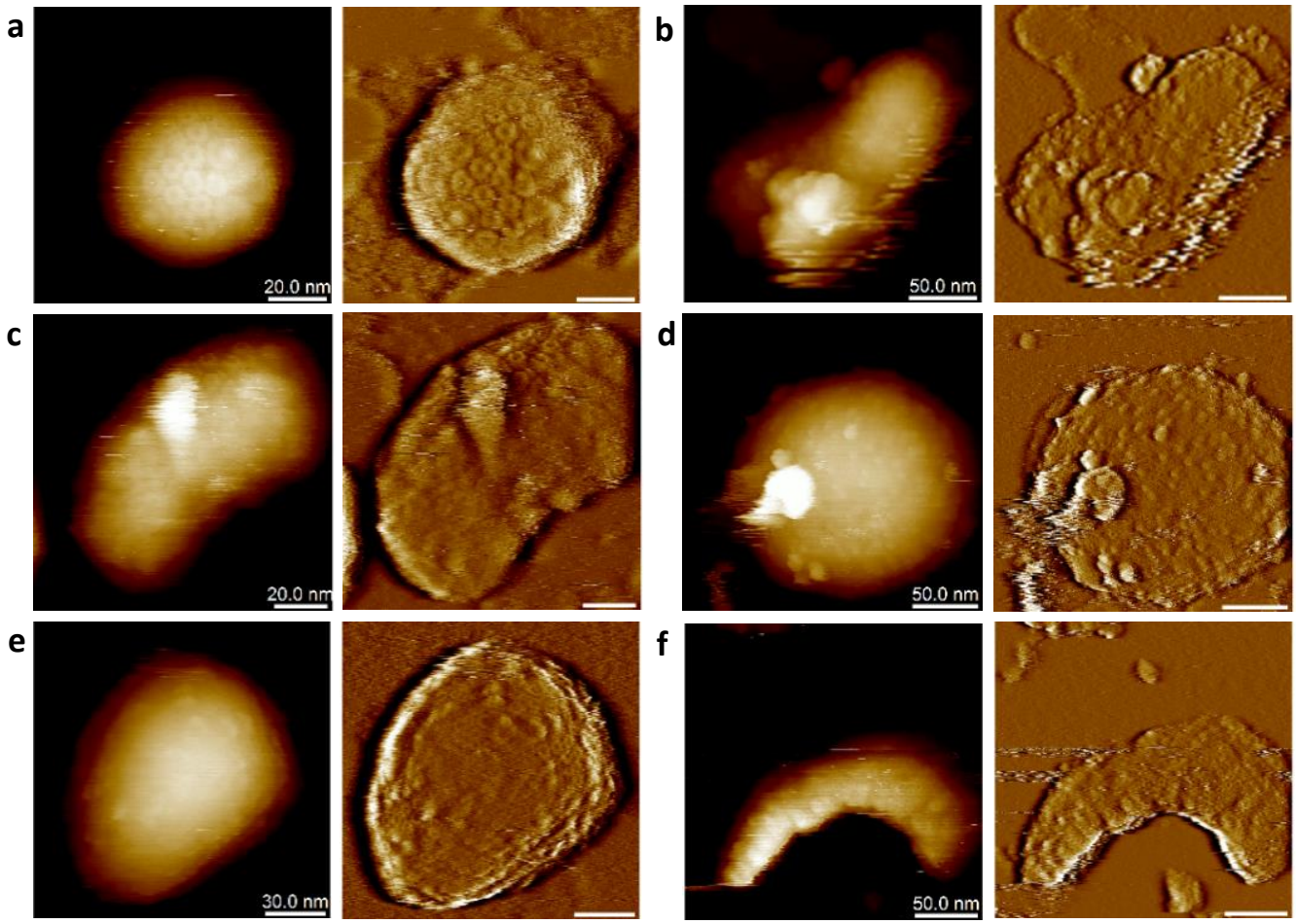


**Supplementary Figure 4. Shapes and sizes of native chromatophore vesicles.** (a), (b), (c), (d), (e), and (f) show images of six differently shaped vesicles with height in the left and high-pass filtered in the right. (a) is a normal sized vesicle, (b) is a vesicle with complex structure, (c) maybe formed by the fusion of two similar sized vesicles, (d) is a large vesicle with an invagination, (e) is a large triangular vesicle, and (f) is a curved tubular vesicle. The respective height range from black to white for the six height images are 45, 35, 65, 65, 85 and 45 nanometers. Scale bars are given in the height images.

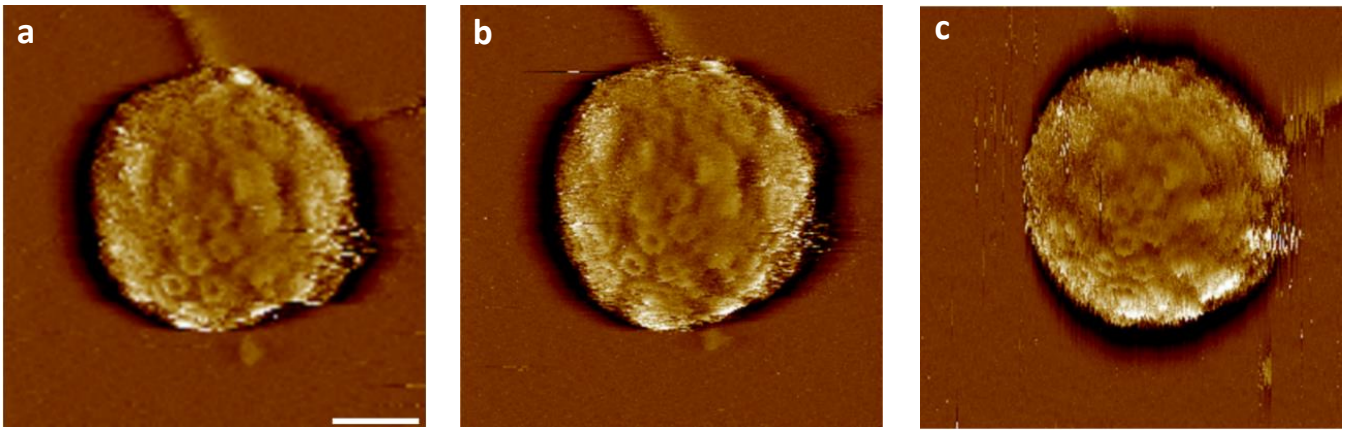


**Supplementary Figure 5. Stability of organization of photosynthetic protein complexes during AFM imaging.** Successive scans with different pixel density and scan angle show an unchanged organization of the protein complexes. (a) is a scan at low pixel density (256X256), (b) is a scan at a higher pixel density (512X512) and (c) is at the same pixel density as (b) but scanned at a 90˚ scan angle. (a), (b) and (c) are high-pass filtered images. The scale bar in (a) represents 20 nm.

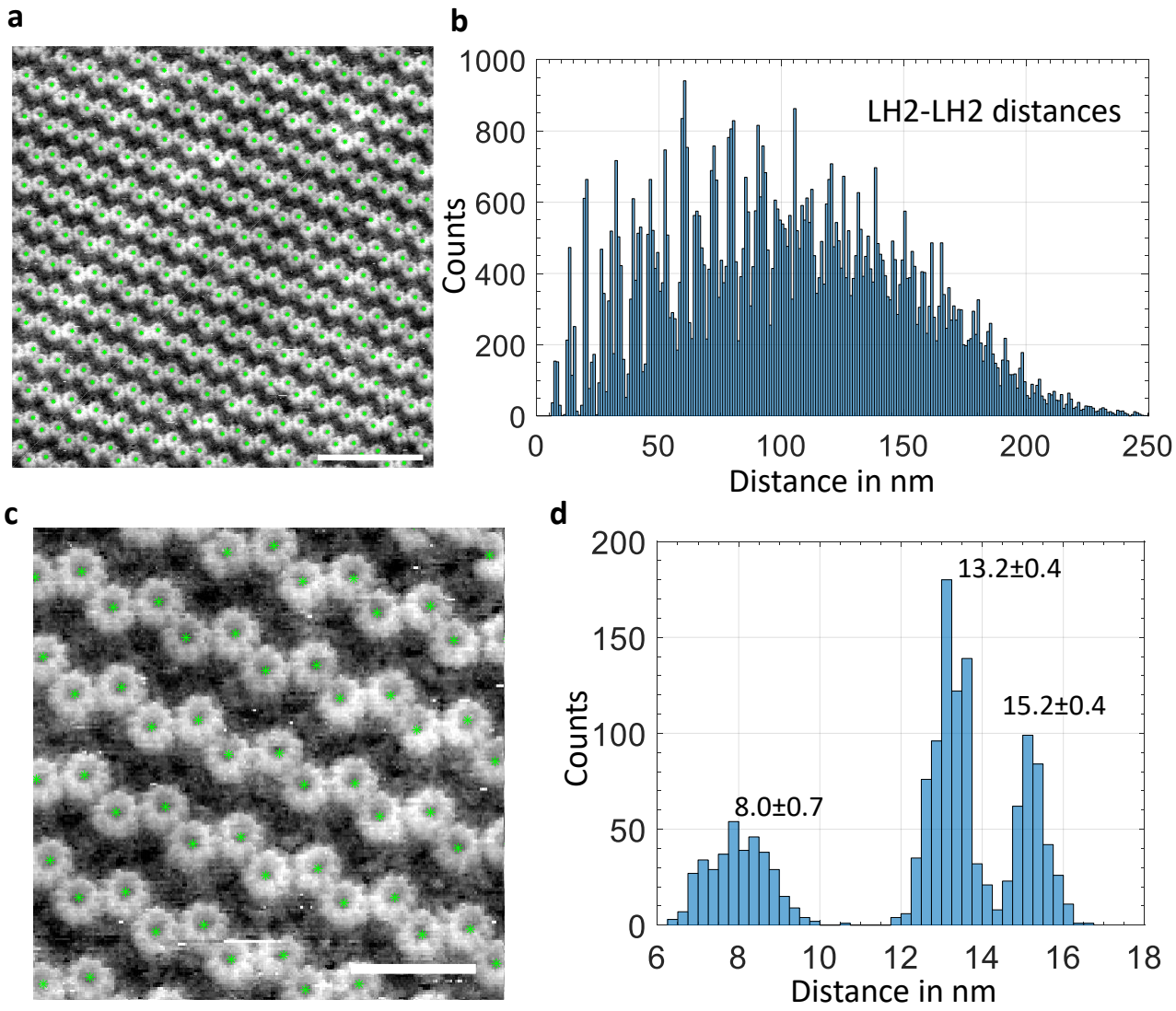


**Supplementary Figure 6. Organization of LH2s in a reconstituted 2D crystal.** (a) is a high resolution AFM image of reconstituted LH2 2D crystal. (b) is the distribution of distances between the centers of each of the LH2 rings showing sharp peaks suggesting crystalline order. (c) shows a zoomed in area of the image (a) where the nine subunits forming the ring are discernible. In (d) the distribution of distances lower than 18 nm showing the nearest neighbor distance distribution. The first peak shows that the LH2 rings are about 8 nm apart. Scale bars in (a) and (c) represent 50 and 20 nm, respectively. Black to white in (a) and (c) is 4 nm.

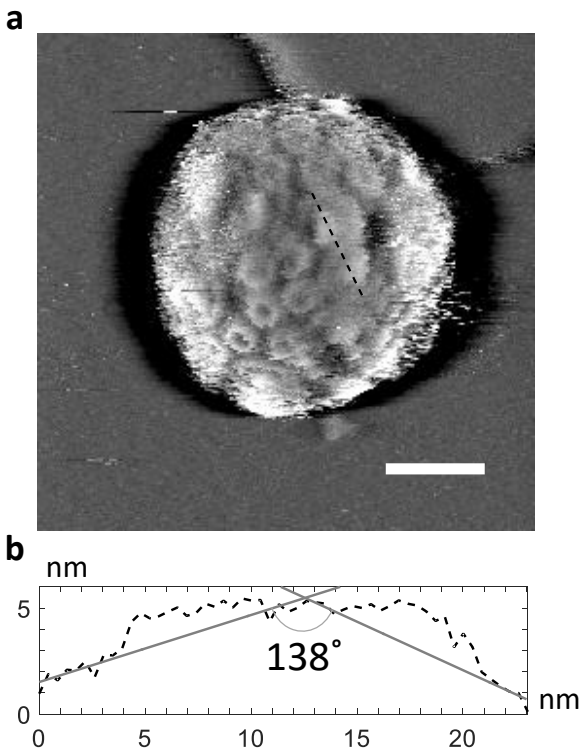


**Supplementary Figure 7. Angle between two halves of the S-shaped RC-LH1-PufX dimer.** (a) shows a high-pass filtered image of a chromatophore where the shape of an S-dimer can be clearly seen. (b) shows a cross-section profile along the S-dimer (black dotted line in (a)) using the unfiltered height image. (b) shows the angle between the two halves to be about 138˚. Scale bar in (a) represents 20 nm.

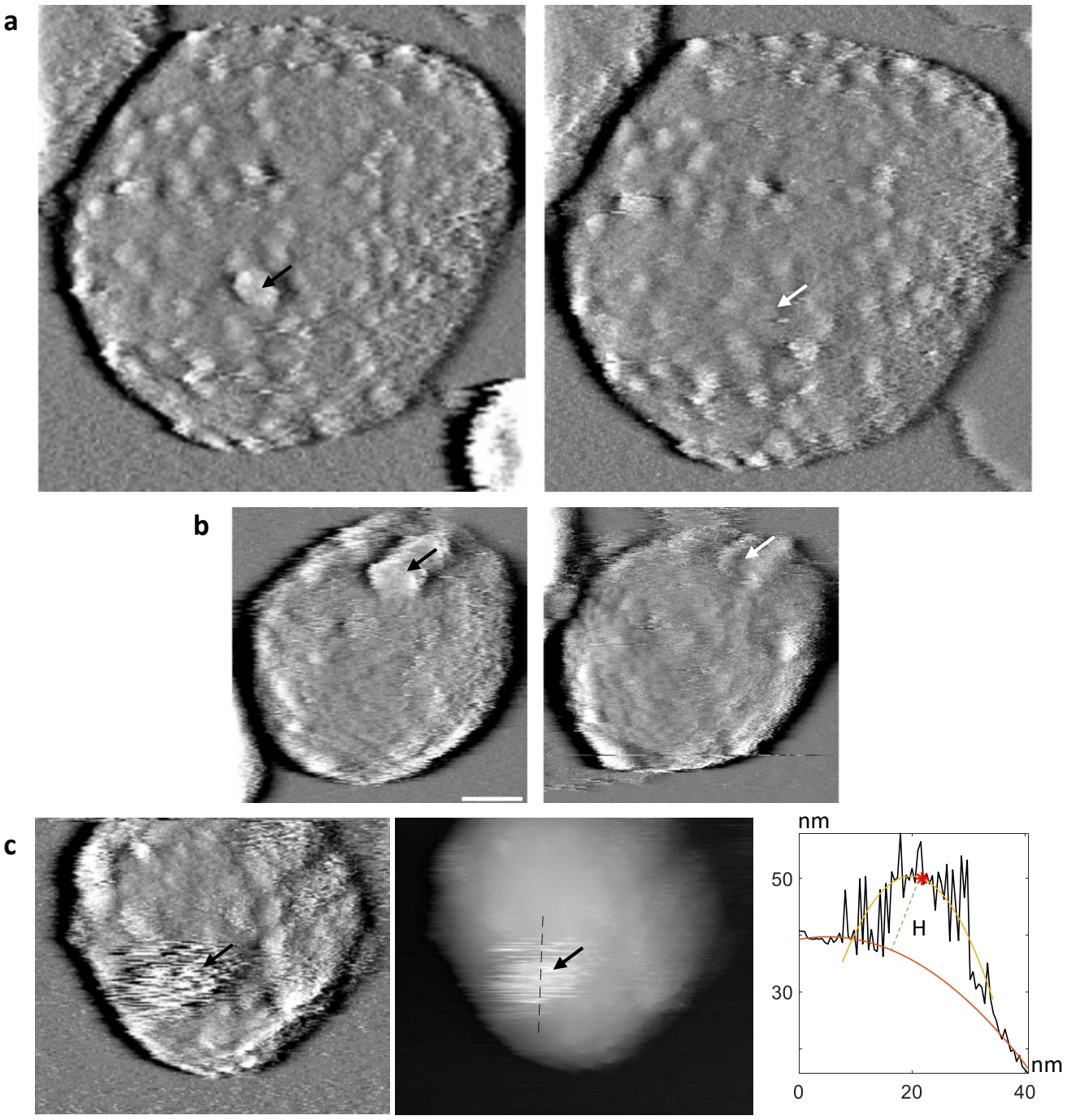


**Supplementary Figure 8. ATPases in chromatophore vesicles.** The black arrows in (a), (b) (left) point towards the ATPases in chromatophores which are lost in later scans (shown by white arrows, right). In (a) the ATPase is surrounded by core complexes. In (b), the ATPase is near the edge of the chromatophore and the LH2 rings surrounding it can be clearly seen. (c) shows an AFM image of a chromatophore fixed with 1% glutaraldehyde to prevent the detachment of ATPase (high-pass filtered (left), height (center)). The black arrow points towards the ATPase while the cross-section along the dotted black line is shown in the right. Red (..) and yellow (..) curves show the quadratic fits to the lipid background and the ATPase respectively. The green dotted line (- -) shows the maximum distance between the ATPase fit and the membrane fit and this distance is taken as height (H) of the ATPase which is 13.8 nm. The red star (*) labels the highest point on the ATPase fit. All images have the same scale and scale bar in (b) represents 20 nm.

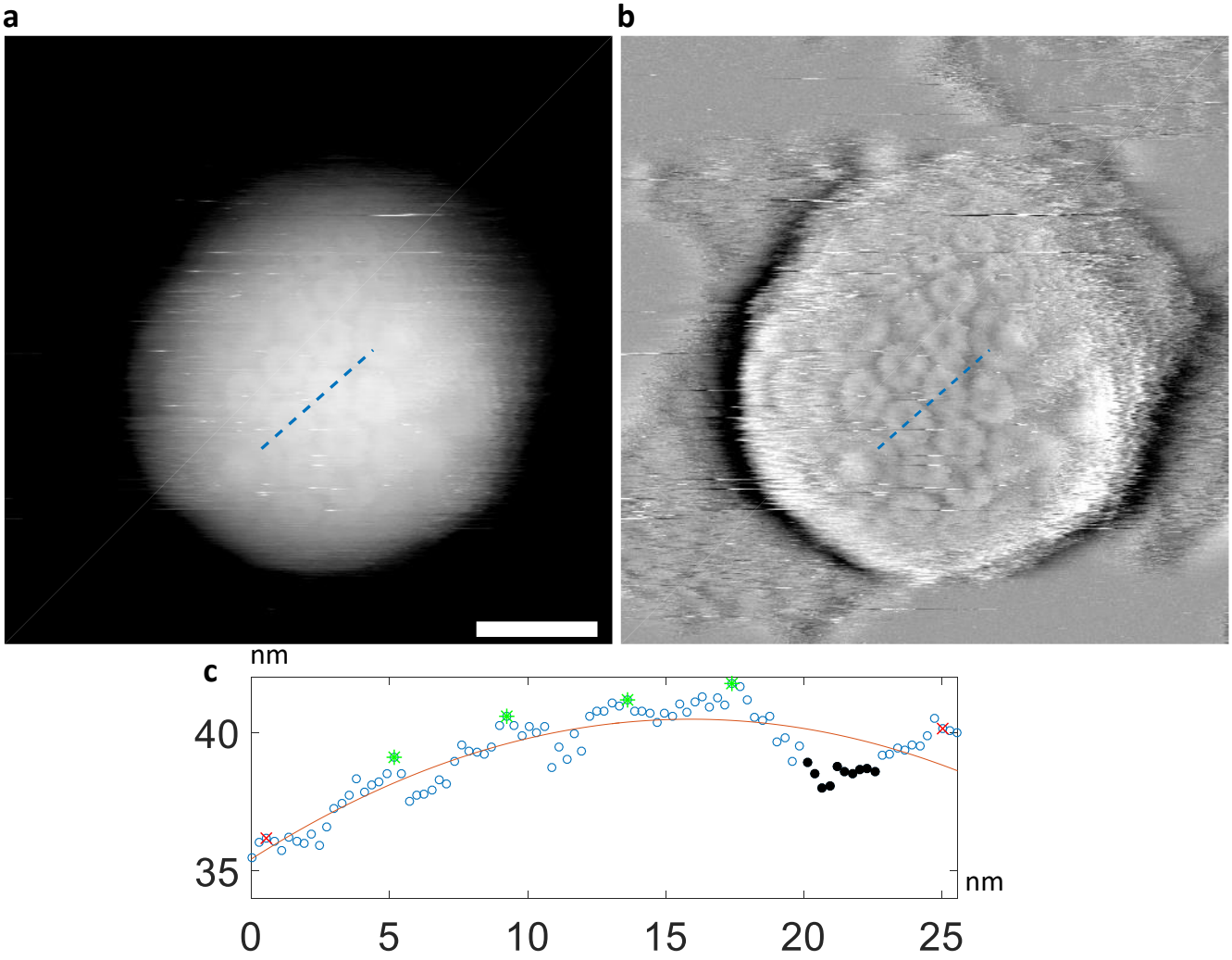


**Supplementary Figure 9. Protrusion heights of LH1 and LH2 proteins above the lipid membrane.** **(**a) shows a height image of the chromatophore with cross-section line starting on top of the LH1 ring of one core complex, passing through two LH2 rings and empty lipid space, and finally ending on top of the LH1 ring of a second core complex. (b) shows the same profile over a high-pass filtered image with improved contrast. (c) shows the heights of the pixels along the profile (o) fit with a quadratic (-) and the fit is taken as the background. The LH1s (x) and LH2s (*) protrude approximately 0.8 nm and 1 nm above the background respectively while the lipid bilayer (marked by **o**) is approximately 1.3 nm below the background in the above profile. So for this cross-sectional profile the LH1s and LH2s protrude 2.1 nm and 2.3 nm above the lipid bilayer. To get the approximate heights of LH1s, LH2s and the lipid bilayer from the background, the average of the shortest distances of the pixels marked with x, * and **o** were calculated from the background fit. Scale bar in (a) represents 20 nm. Black to white in (a) is 45 nm.

## Supporting Information References


1. San Paulo, A.; García, R. Tip-Surface Forces, Amplitude, and Energy Dissipation in Amplitude-Modulation (Tapping Mode) Force Microscopy. *Phys. Rev. B* **2001,** *64*, 193411.
2. Rodrıguez, T. R.; García, R. Tip Motion in Amplitude Modulation (Tapping-Mode) Atomic-Force Microscopy: Comparison between Continuous and Point-Mass Models. *Appl. Phys. Lett.* **2002,** *80*, 1646-1648.
3. Walters, D.; Cleveland, J.; Thomson, N.; Hansma, P.; Wendman, M.; Gurley, G.; Elings, V. Short Cantilevers for Atomic Force Microscopy. *Rev. Sci. Instrum.* **1996,** *67*, 3583-3590.
4. Giessibl, F. J.; Bielefeldt, H.; Hembacher, S.; Mannhart, J. Calculation of the Optimal Imaging Parameters for Frequency Modulation Atomic Force Microscopy. *Appl. Surf. Sci.* **1999,** *140*, 352-357.
5. Israelachvili, J. N. *Intermolecular and Surface Forces: Revised Third Edition*. Academic press: 2011.